

# An Uncertain Future: Forecasting from Static Images Using Variational Autoencoders

Jacob Walker<sup>(✉)</sup>, Carl Doersch, Abhinav Gupta, and Martial Hebert

Carnegie Mellon University, Pittsburgh, USA  
{jwalker,cdoersch,abhinavg,hebert}@cs.cmu.edu

**Abstract.** In a given scene, humans can easily predict a set of immediate future events that might happen. However, pixel-level anticipation in computer vision is difficult because machine learning struggles with the ambiguity in predicting the future. In this paper, we focus on predicting the dense trajectory of pixels in a scene—what will move in the scene, where it will travel, and how it will deform over the course of one second. We propose a conditional variational autoencoder as a solution to this problem. In this framework, direct inference from the image shapes the distribution of possible trajectories while latent variables encode information that is not available in the image. We show that our method predicts events in a variety of scenes and can produce multiple different predictions for an ambiguous future. We also find that our method learns a representation that is applicable to semantic vision tasks.

**Keywords:** Generative models · Variational autoencoders · Scene understanding · Action forecasting

## 1 Introduction

Visual prediction is one of the most fundamental and difficult tasks in computer vision. For example, consider the woman in the gym in Fig. 1. We as humans, given the context of the scene and her sitting pose, know that she is probably performing squat exercises. However, going beyond the action label and predicting the future leads to multiple, richer possibilities. The woman might be on her way up and will continue to go up, or she might be on the way down and continue to descend further. Those motion trajectories might not be exactly vertical, as the woman might lean or move her arms back as she ascends. While there are multiple possibilities, the space of possible futures is significantly smaller than the space of all possible visual motions. For example, we know she is not going to walk forward, she is not going to perform an incoherent action such as a head-bob, and her torso will likely remain in one piece. In this paper, we propose to develop a generative framework which, given a static input image, outputs the space of possible future actions. The key here is that our model characterizes the whole distribution of future states and can be used to sample multiple possible future events.

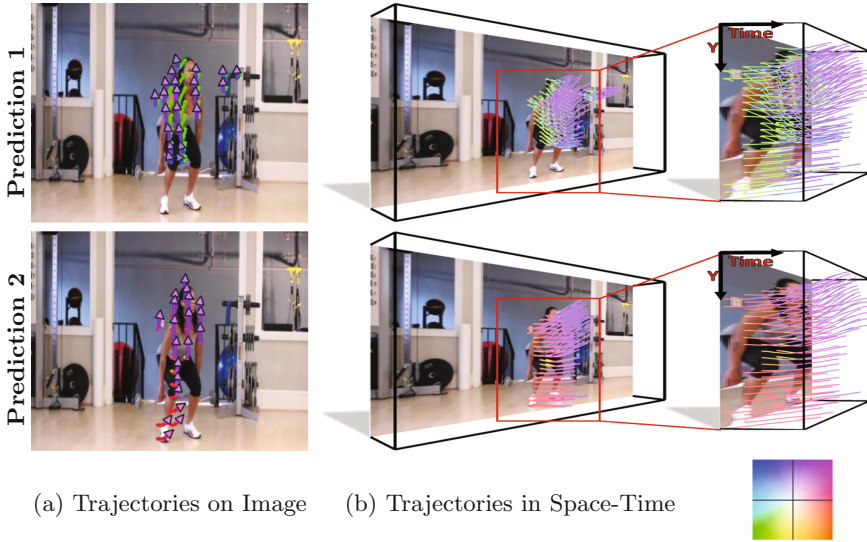


**Fig. 1.** Consider this picture of a woman in the gym—she could move up or down. Our framework is able to predict multiple correct one-second motion trajectories given the scene. The directions of the trajectories at each point in time are color-coded according to the square on the right [2]. On the left is the projection of the trajectories on the image plane. The right diagram shows the complexity of the predicted motions in space time. Best seen in our [videos](#). (Color figure online)

Even if we acknowledge that our algorithm must produce a distribution over many possible predictions, it remains unclear what is the output space of futures the algorithm should be capable of predicting. An ideal algorithm would predict everything that might be relevant to a human or robot interacting with the scene, but this is far too complicated to be feasible with current methods. A more tractable approach is to predict dense trajectories [33], which are simpler than pixels but still capture most of a video’s content. While this representation is intuitive, the output space is high dimensional and hard to parametrize, an issue which forced [33] to use a Nearest Neighbor algorithm and transfer raw trajectories. Unsurprisingly, the algorithm is computationally expensive and fails on testing images which do not have globally similar training images. Many approaches try to simplify the problem, either by using some semantic form of prediction [20], predicting agent-based trajectories in a restricted domain [30], or just predicting the optical flow to the next frame [23,31]. However, each of these representations compromise the richness of output in either the spatial domain (agent-based), the temporal domain (optical flow), or both (semantic). Therefore, the vision community has recently pushed back and directly attacked the problem of full blown visual prediction: recent works have proposed predicting pixels [24,28] or the high dimensional fc7 features [29] themselves. However, these approach suffer from a number of drawbacks. Notably, the output space

is high dimensional and it is difficult to encode constraints on the output space, e.g., pixels can change colors every frame. There is also an averaging effect of multiple possible predictions which leads to blurry predictions.

In this paper, we propose to address these challenges. We propose to revisit the idea of predicting dense trajectories at each and every pixel using a feed-forward Convolutional Network. Using dense trajectories restricts the output space dramatically which allows our algorithm to learn robust models for visual prediction with the available data. However, the dense trajectories are still high-dimensional, and the output still has multiple modes. In order to tackle these challenges, we propose to use variational autoencoders to learn a low-dimensional latent representation of the output space conditioned on an input image. Specifically, given a single frame as input, our *conditional* variational auto-encoder outputs a mapping from noise variables—sampled from a normal distribution  $\mathcal{N}(0, 1)$ —to output trajectories at every pixel. Thus, we can naively sample values of the latent variables and pass them through the mapping in order to sample different predicted trajectories from the inferred conditional distribution. Unlike other applications of variational autoencoders that generate outputs a priori [10, 13, 14], we focus on generating them *given the image*. Conditioning on the image is a form of inference, restricting the possible motions based on object location and scene context. Sampling latent variables during test time then allows us to explore the space of possible actions in the given scene.

**Contributions:** Our paper makes three contributions. First, we demonstrate that prediction of dense pixel trajectories is a plausible approach to general, non-semantic, self-supervised visual prediction. Second, we propose a conditional variational auto-encoder as a solution to this problem, a model that performs inference on an image by conditioning the distribution of possible movements on a scene. Third, we show that our model is capable of learning representations for various recognition tasks with less data than conventional approaches.

## 2 Background

There have been two main thrusts in recent years concerning visual activity forecasting. The first is an unsupervised, largely non-semantic approach driven by large amounts of data. These methods often focus on predicting low level features such as pixels or the motion of pixels. One early approach used nearest-neighbors, making predictions for an image by matching it to frames in a large collection of videos and transferring the associated motion tracks [33]. An improvement to this approach used dense-SIFT correspondence to align the matched objects in two images [21]. This form of nearest-neighbors, however, relied on finding global matches to an image’s entire contents. One way this limitation has been addressed is by breaking the images into smaller pieces based on mid-level discriminative patches [30]. Another way is to treat prediction as a regression problem and use standard machine learning, but existing algorithms struggle to capture the complexity of real videos. Some works simplify the problem to predicting optical flow between pairs of frames [23]. Recently, more powerful deep

learning approaches have improved on these results on future [31] and current [5] optical flow. Some works even suggest that it may be possible to use deep networks to predict raw pixels [24, 28]. However, even deep networks still struggle with underfitting in this scenario. Hence, [29] considered predicting the top-level CNN features of future frames rather than pixels. Since predicting low level features such as pixels is often so difficult, other works have focused on predicting more semantic information. For example, some works break video sequences into discrete actions and attempt to detect the earliest frames in an action in order to predict the rest [11]. Others predict labeled human walking trajectories [15] or object trajectories [22] in restricted domains. Finally, supervised learning has also been used to model and forecast labeled human-human [12, 20], and human-object [7, 16] interactions.

A key contribution of our approach is that we explicitly model a distribution over possible futures in the high-dimensional, continuous output space of trajectories. That is, we build a generative model over trajectories given an image. While previous approaches to forecasting have attempted to address multimodality [15, 29–31], we specifically rely on the recent generative model framework of variational autoencoders (VAEs) to solve the problem. VAEs have already shown promise in a number of domains involving generating pixels, including handwritten digits [14, 26], faces [14, 25], house numbers [13], CIFAR images [10], and even face pose [19]. Our work shows that VAEs extend to the novel domain of motion prediction in the form of trajectories.

Our approach has multiple advantages over previous works. First, our approach requires no human labeling. While [22] also predicted long-term motion of objects, it required manual labels. Second, our approach is able to predict for a relatively long period of time: one second. While [23, 31] needed no human labeling, they only focused on predicting motion for the next instant frame. While [31] did consider long-term optical flow as a proof of concept, they did not tackle the possibility of multiple potential futures. Finally, our algorithm predicts from a single image—which may enable graphics applications that involve animating still photographs—while many earlier works require video inputs [24, 28].

### 3 Algorithm

We aim to predict the motion trajectory for each and every pixel in a static, RGB image over the course of one second. Let  $X$  be the image, and  $Y$  be the full set of trajectories. The raw output space for  $Y$  is very large— $320 \times 240 \times 30 \times 2$  for a  $320 \times 240$  image at 30 frames per second—and it is continuous. We can simplify the output space somewhat by encoding the trajectories in the frequency spectrum in order to reduce dimensionality. However, a more important difficulty than raw data size is that the output space is not unimodal; an image may have multiple reasonable futures.

### 3.1 Model

A simple regressor—even a deep network with millions of parameters—will struggle with predicting one-second motion in a single image as there may be many plausible outputs. Our architecture augments the simple regression model by adding another input  $z$  to the regressor (shown in Fig. 2(a)), which can account for the ambiguity. At test time,  $z$  is random Gaussian noise: passing an image as input and sampling from the noise variable allows us to sample from the model’s posterior given the image. That is, if there are multiple possible futures given an image, then for each possible future, there will be a different set of  $z$  values which map to that future. Furthermore, the likelihood of sampling each possible future will be proportional to the likelihood of sampling a  $z$  value that maps to it. Note that we assume that the regressor—in our case, a deep neural network—is capable of encoding dependencies between the output trajectories. In practice, this means that if two pixels need to move together even if the direction of motion is uncertain, then they can simply be influenced by the same dimension of the  $z$  vector.

### 3.2 Training by “Autoencoding”

It is straightforward to sample from the posterior at test time, but it is much less straightforward to train a model like this. The problem is that given some ground-truth trajectory  $Y$ , we cannot directly measure the probability of the trajectory given an image  $X$  under a given model; this prevents us from performing gradient descent on this likelihood. It is in theory possible to estimate this conditional likelihood by sampling a large number of  $z$  values and constructing a Parzen window estimate using the resulting trajectories, but this approach by itself is too costly to be useful.

Variational Autoencoders [3, 10, 13, 14] make this approach tractable. The key insight is that the vast majority of samples  $z$  contribute almost nothing to the overall likelihood of  $Y$ . Hence, we should instead focus only on those values of  $z$  that are likely to produce values close to  $Y$ . We do this by adding another pathway  $Q$ , as shown in Fig. 2(b), which is trained to map the output  $Y$  to the values of  $z$  which are likely to produce them. That is,  $Q$  is trained to “encode”  $Y$  into the latent  $z$  space such that the values can be “decoded” back to the trajectories. The entire pipeline can be trained end-to-end using reconstruction error. An immediate objection one might raise is that this is essentially “cheating” at training time: the model sees the values that it is trying to predict, and may just copy them to the output. To prevent the model from simply copying, we force the encoding to be lossy. The  $Q$  pathway does not produce a single  $z$ , but instead, produces a distribution over  $z$  values, which we sample from before decoding the trajectories. We then directly penalize the information content in this distribution, by penalizing the  $\mathcal{KL}$ -divergence between the distribution produced by  $Q$  and the trajectory-agnostic  $\mathcal{N}(0, 1)$  distribution. The model is thereby encouraged to extract as much information as possible from the input image before relying on encoding the trajectories themselves. Surprisingly, this formulation is

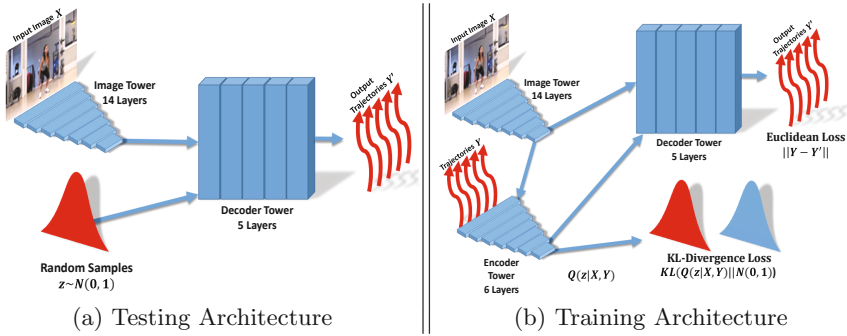


**Fig. 2.** Overview of the architecture. During training, the inputs to the network include both the image and the ground truth trajectories. A variational autoencoder encodes the joint image and trajectory space, while the decoder produces trajectories depending both on the image information as well as output from the encoder. During test time, the only inputs to the decoder are the image and latent variables sampled from a normal distribution.

a very close approximation to maximizing the posterior likelihood  $P(Y|X)$  that we are interested in. In fact, if our encoder pathway  $Q$  can estimate the exact distribution of  $z$ 's that are likely to generate  $Y$ , then the approximation is exact.

### 3.3 The Conditional Variational Autoencoder

We now show mathematically how to perform gradient descent on our conditional VAE. We first formalize the model in Fig. 2(a) with the following formula:

$$Y = \mu(X, z) + \epsilon \tag{1}$$

where  $z \sim \mathcal{N}(0, 1)$ ,  $\epsilon \sim \mathcal{N}(0, 1)$  are both white Gaussian noise. We assume  $\mu$  is implemented as a neural network.

Given a training example  $(X_i, Y_i)$ , it is difficult to directly infer  $P(Y_i|X_i)$  without sampling a large number of  $z$  values. Hence, the variational “autoencoder” framework first samples  $z$  from some distribution different from  $\mathcal{N}(0, 1)$  (specifically, a distribution of  $z$  values which are likely to give rise to  $Y_i$  given  $X_i$ ), and uses that sample to approximate  $P(Y|X)$  in the following way. Say that  $z$  is sampled from an arbitrary distribution  $z \sim Q$  with p.d.f.  $Q(z)$ . By Bayes rule, we have:

$$E_{z \sim Q} [\log P(Y_i|z, X_i)] = E_{z \sim Q} [\log P(z|Y_i, X_i) - \log P(z|X_i) + \log P(Y_i|X_i)] \tag{2}$$

Rearranging the terms and subtracting  $E_{z \sim Q} \log Q(z)$  from both sides:

$$\log P(Y_i|X_i) - E_{z \sim Q} [\log Q(z) - \log P(z|X_i, Y_i)] = E_{z \sim Q} [\log P(Y_i|z, X_i) + \log P(z|X_i) - \log Q(z)] \tag{3}$$

Note that  $X_i$  and  $Y_i$  are fixed, and  $Q$  is an arbitrary distribution. Hence, during training, it makes sense to choose a  $Q$  which will make  $E_{z \sim Q}[\log Q(z) - \log P(z|X_i, Y_i)]$  (a  $\mathcal{KL}$ -divergence) small, such that the right hand side is a close approximation to  $\log P(Y_i|X_i)$ . Specifically, we set  $Q = \mathcal{N}(\mu'(X_i, Y_i), \sigma'(X_i, Y_i))$  for functions  $\mu'$  and  $\sigma'$ , which are also implemented as neural networks, and which are trained alongside  $\mu$ . We denote this p.d.f. as  $Q(z|X_i, Y_i)$ . We can rewrite some of the above expectations as  $\mathcal{KL}$ -divergences to obtain the standard variational equality:

$$\begin{aligned} \log P(Y_i|X_i) - \mathcal{KL}[Q(z|X_i, Y_i)||P(z|X_i, Y_i)] \\ = E_{z \sim Q}[\log P(Y_i|z, X_i)] - \mathcal{KL}[Q(z|X_i, Y_i)||P(z|X_i)] \end{aligned} \quad (4)$$

We compute the expected gradient with respect to only the right hand side of this equation—the parameters of our network that constitute  $P$  and  $Q$ , so that we can perform gradient ascent and maximize both sides. Note that this means our algorithm is accomplishing two things simultaneously: it is maximizing the likelihood of  $Y$  while also training  $Q$  to approximate  $P(z|X_i, Y_i)$  as well as possible. Assuming a high capacity  $Q$  which can accurately model  $P(z|X_i, Y_i)$ , this second  $\mathcal{KL}$ -divergence term will tend to 0, meaning that we will be directly optimizing the likelihood of  $Y$ . To perform the optimization, first note that our model in Eq. 1 assumes  $P(z|X_i) = \mathcal{N}(0, 1)$ , i.e.,  $z$  is independent of  $X$  if  $Y$  is unknown. Hence, the  $\mathcal{KL}$ -divergence may be computed using a closed form expression, which is differentiable with respect to the parameters of  $\mu'$  and  $\sigma'$ . We can approximate the expected gradient of  $\log P(Y_i|z, X_i)$  by sampling values of  $z$  from  $Q$ . The main difficulty, however, is that the distribution of  $z$  depends on the parameters of  $\mu'$  and  $\sigma'$ , which means we must backprop through the apparently non-differentiable sampling step. We use the “reparameterization trick” [14, 25] to make sampling differentiable. Specifically, we set  $z_i = \mu'(X_i, Y_i) + \eta \circ \sigma'(X_i, Y_i)$ , where  $\eta \sim \mathcal{N}(0, 1)$  and  $\circ$  denotes an elementwise product. This makes  $z_i \sim Q$  while allowing the expression for  $z_i$  to be differentiable with respect to  $\mu'$  and  $\sigma'$ .

### 3.4 Architecture

Our conditional variational autoencoder requires neural networks to compute three separate functions:  $\mu(X, z)$  which comprises the “decoder” distribution of trajectories given images ( $P(Y|X, z)$ ), and  $\mu'$  and  $\sigma'$  which comprise the “encoder” distribution ( $Q(z|X, Y)$ ). However, much of the computation can be shared between these functions: all three depend on the image information, and both  $\mu'$  and  $\sigma'$  rely on exactly the same information (image and trajectories). Hence, we can share computation between them. The resulting network can be summarized as three “towers” of neural network layers, as shown in Fig. 2. First, the “image” tower processes each image, and is used to compute all three quantities. Second is the “encoder” tower, which takes input from the “image” tower as well as the raw trajectories, and has two tops, one for  $\mu'$  and one for  $\sigma'$ , which implements the  $Q$  distribution. This tower is discarded at test time. Third is the “decoder” tower, which takes input from the “image” tower as well

as the samples for  $z$ , either produced by the “encoder” tower (training time) or random noise (test time). All towers are fully-convolutional. The remainder of this section details the design of these three towers.

**Image Tower:** The first, the image data tower, receives only the  $320 \times 240$  image as input. The first five layers of the image tower are almost identical to the traditional AlexNet [18] architecture with the exception of extra padding in the first layer (to ensure that the feature maps remain aligned to the pixels). We remove the fully connected layers, since we want the network to generalize across translations of the moving object. We found, however, that 5 convolutional layers is too little capacity, and furthermore limits each unit’s receptive field to too small a region of the input. Hence, we add nine additional 256-channel convolutional layers with local receptive fields of 3. To simplify notation, denote  $C(k, s)$  as a convolutional layer with number of filters  $k$  and receptive field size  $s$ . Denote  $LRN$  as a Local Response Normalization, and  $P$  as a max-pooling layer. Let  $\rightarrow C(k, s)_i \rightarrow C(k, s)_{i+1}$  denote a series of stacked convolutional layers with the same kernel size and receptive field size. This results in a network described as:  $C(96, 11) \rightarrow LRN \rightarrow P \rightarrow C(256, 5) \rightarrow LRN \rightarrow P \rightarrow C(384, 3) \rightarrow C(384, 3) \rightarrow C(256, 3)_1 \rightarrow C(256, 3)_2 \dots \rightarrow C(256, 3)_{10}$ .

**Encoder Tower:** We begin with the frequency-domain trajectories as input and downsample them spatially such that they can be concatenated with the output of the image tower. The encoder tower takes this tensor as input and processes them with five convolutional layers similar to AlexNet, although the input consists of output from the image tower and trajectory data concatenated into one input data layer. After the fifth layer, two additional convolutional layers compute  $\mu'$  and  $\sigma'$ . Empirically, we found that predictions are improved if the latent variables are independent of spatial location: that is, we average-pool the outputs of these convolutional layers across all spatial locations. We use eight latent variables to encode the normalized trajectories across the entire image. Empirically, a larger number of latent variables seemed to overfit. At training time, we can sample the  $z$  input to the decoder tower as  $z = \mu' + \eta \circ \sigma'$  where  $\eta \sim \mathcal{N}(0, 1)$ .  $\mu'$  and  $\sigma'$  also feed into a loss layer which computes the  $\mathcal{KL}$  divergence to the  $\mathcal{N}(0, 1)$  distribution. This results in a network described as:  $C(96, 11) \rightarrow LRN \rightarrow P \rightarrow C(256, 5) \rightarrow LRN \rightarrow P \rightarrow C(384, 3) \rightarrow C(384, 3) \rightarrow C(256, 3) \rightarrow C(8, 1) \times 2$ .

**Decoder Tower:** We replicate the sampled  $z$  values across spatial dimensions and multiply them with the output of the image tower with an offset. This serves as input to four additional 256-channel convolutional layers which constitute the decoder. The fifth convolutional layer is the predicted trajectory space over the image. This can be summarized by:  $C(256, 3)_1 \rightarrow C(256, 3)_2 \dots \rightarrow C(256, 3)_4 \rightarrow C(10, 3)$ . This output is over a coarse resolution—a dimensionality of  $16 \times 20$  pixels and a 10 vector at each pixel describing its compressed trajectory in the frequency domain. The simplest loss layer for this is the pure Euclidean loss, which corresponds to log probability according to our model (Eq. 1). However, we empirically find much faster convergence if we split this loss into two



components: one is the *normalized* version of the trajectory, and the other is the magnitude (with a separate magnitude for horizontal and vertical motions). Because the amount of absolute motion varies considerably between images—and in particular, some action categories have much less motion overall—the normalization is required so that the learning algorithm gives equal weight to each image. The total loss function is therefore:

$$L(X, Y) = \|Y_{\text{norm}} - \hat{Y}_{\text{norm}}\|^2 + \|M_x - \hat{M}_x\|^2 + \|M_y - \hat{M}_y\|^2 + \mathcal{KL}[Q(z|X, Y) \| \mathcal{N}(0, 1)] \quad (5)$$

where  $Y$  represents trajectories,  $X$  is the image,  $M_i$  are the global magnitudes, and  $\hat{Y}$ ,  $\hat{M}_i$  are the corresponding estimates by our network. The last term is the KL-divergence loss of the autoencoder. We find empirically that it also helps convergence to separate both the latent variables and the decoder pathways that generate  $\hat{Y}_{\text{norm}}$  from the ones that generate  $\hat{M}$ .

**Coarse-to-Fine:** The network as described above predicts trajectories at a stride of 16, i.e., at 1/16 the resolution of the input image. This is often too coarse for visualization, but training directly on higher-resolution outputs is slow and computationally wasteful. Hence, we only begin training on higher-resolution trajectories after the network is close to convergence on lower resolution outputs. We ultimately predict three spatial resolutions—1/16, 1/8, and 1/4 resolution—in a cascade manner similar to [6]. The decoder outputs directly to a  $16 \times 20$  resolution. For additional resolution, we upsample the underlying feature map and concatenate it with the conv4 layer of the image tower. We pass this through 2 additional convolution layers,  $D = C(256, 5) \rightarrow C(10, 5)$ , to predict at a resolution of  $32 \times 40$ . Finally, we upsample this feature layer  $D$ , concatenate it with the conv1 layer of the image tower, and send it through one last layer of  $C(10, 5)$  for a final output of  $64 \times 80$ .

## 4 Experiments

Because almost no prior work has focused on motion prediction beyond the timescale of optical flow, there are no established metrics or datasets for the task. For our quantitative evaluations, we chose to train our network on videos from the UCF101 dataset [27]. Although there has been much recent progress on this dataset from an action recognition standpoint, pixel-level prediction on even the UCF101 dataset has proved to be non-trivial [24, 28].

Because the scene diversity is low in this dataset, we utilized as much training data as possible, i.e., all the videos except for a small hold out set for every action. We sampled every 3rd frame for each video, creating a training dataset of approximately 650,000 images. Testing data for quantitative evaluation came from the testing portion of the THUMOS 2015 challenge dataset [9]. The UCF101 dataset is the training dataset for the THUMOS challenge, and thus THUMOS is a relevant choice for the testing set. We randomly sampled 2800 frames and their corresponding trajectories for our testing data. We will make this list of frames

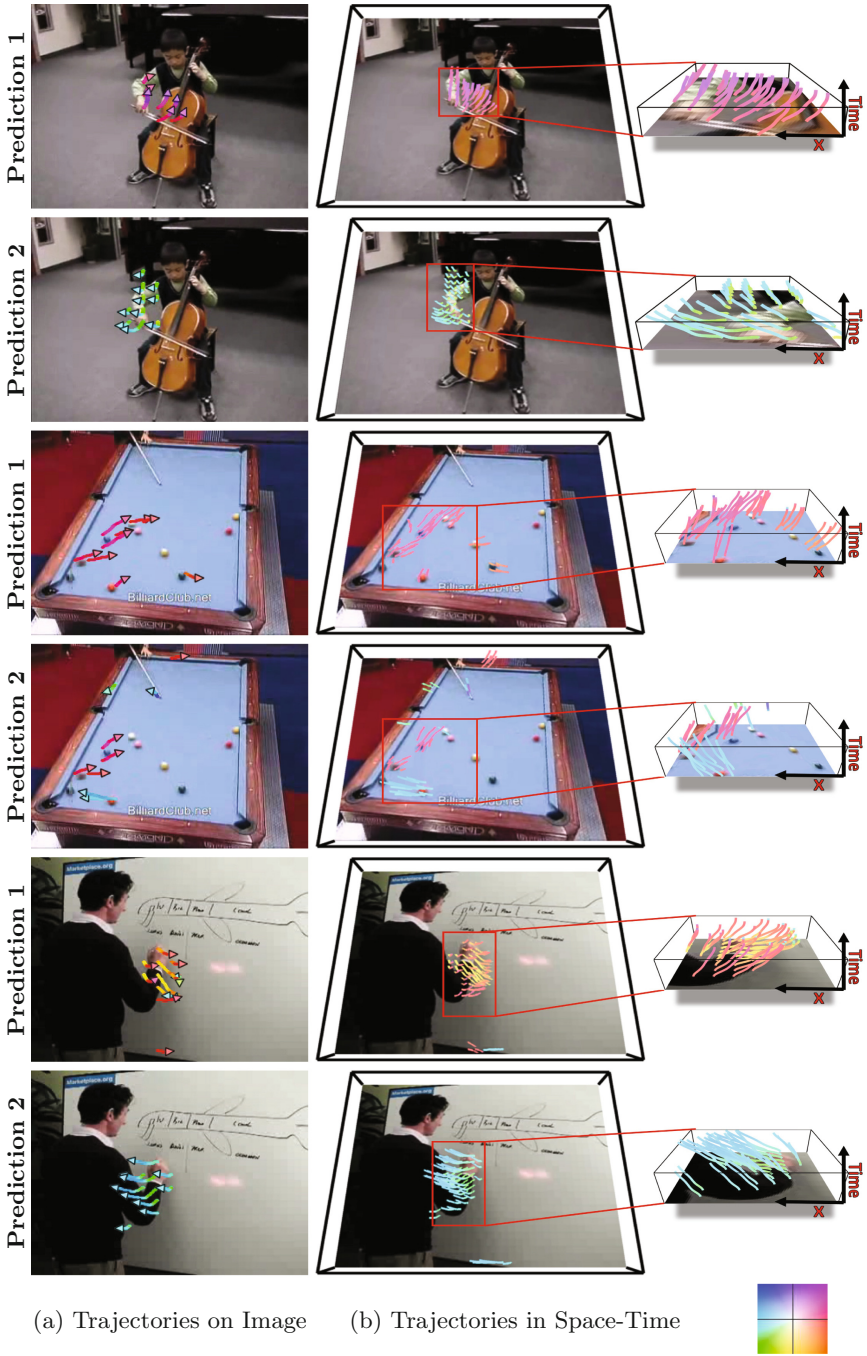


**Fig. 3.** Predictions of our model based on clustered samples. On the right is a full view of two predicted motions in 3D space-time; on the left is the projection of the trajectories onto the image plane. Best seen in our [videos](#).

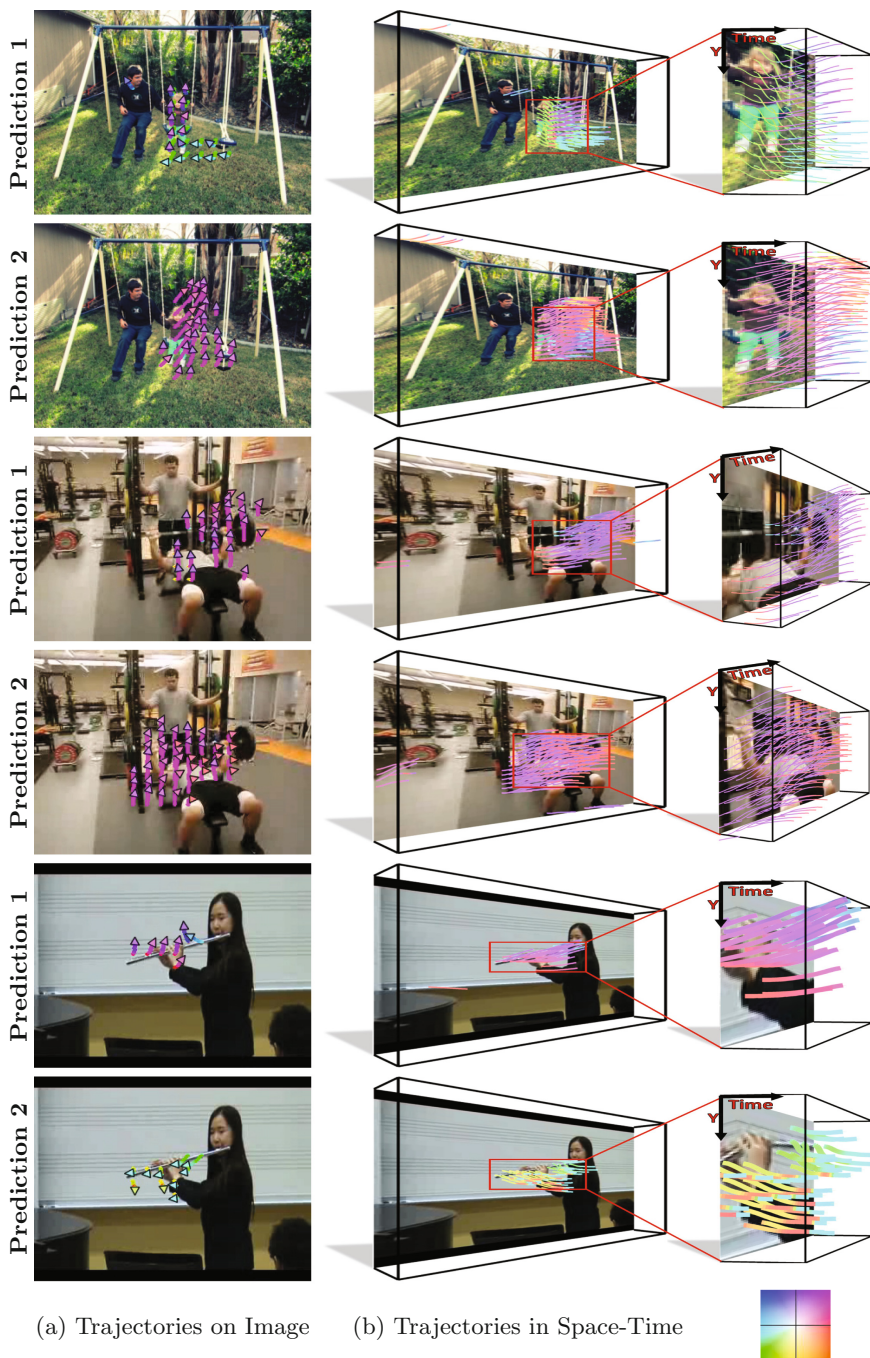


**Fig. 4.** Predictions of our model based on clustered samples. On the right is a full view of two predicted motions in 3D space-time; on the left is the projection of the trajectories onto the image plane. Best seen in our [videos](#).

publicly available. We use two baselines for trajectory prediction. The first is a direct regressor (i.e., no autoencoder) for trajectories using the same layer architecture from the image data tower. The second baseline is the optical flow prediction network from [31], which was trained on the same dataset. We simply extrapolate the predicted motions of the network over one second. Choosing an effective metric for future trajectory prediction is challenging since the problem is inherently multi-modal. There might be multiple correct trajectories for every testing instance.

**Log Likelihood Evaluation:** We thus first evaluate our method in the context of generative models: we evaluate whether our method estimates a distribution where the ground truth is highly probable. Namely, given a testing example, we estimate the full conditional distribution over trajectories and calculate the log-likelihood of the ground truth trajectory under our model. For log-likelihood estimation, we construct Parzen window estimates using samples from our network, using a Gaussian kernel. We estimate the optimal bandwidth for the Parzen window via gridsearch on the training data. As the networks were originally trained to optimize over normalized trajectories and magnitude separately, we also separate normalized trajectory from magnitude in the testing data, and we estimate bandwidths separately for normalized trajectories and magnitudes. To evaluate the log-likelihood of the ground truth under our first baseline—the regressor—we treat the regressor’s output as a mean of a multivariate Gaussian distribution. The optical flow network uses a soft-max layer to estimate the per-pixel distribution of motions in the image; we thus take samples of motions using this estimated distribution. We then use the samples to estimate a density function in the same manner as the VAE. For the baselines, we optimize the bandwidth over the testing data in order to obtain an upper bound for the likelihood.

**Closest Samples Evaluation:** As log-likelihood may be difficult to interpret, we use an additional metric for evaluation. While average Euclidean distance over all the samples in a particular image may not be particularly informative, it may be useful to know what was the best sample created by the algorithm. Specifically, given a set number  $n$  of samples per image, we measure the Euclidean distance of the closest sample to the ground truth and average over all the testing images. For a reasonable comparison, it is necessary to make sure that every algorithm has an equal number of chances, so we take precisely  $n$  samples from each algorithm per image. For the optical flow baseline [31], we can take samples from the underlying softmax probability distribution. For the regressor, we sample from a multivariate Gaussian centered at the regressor output and use the bandwidth parameters estimated from grid-search.

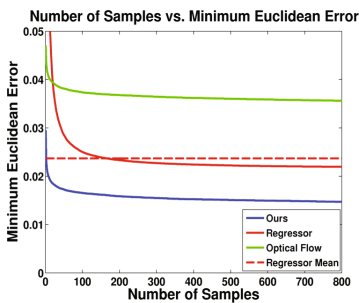
## 4.1 Quantitative Results

In Fig. 5(a), we show our log-likelihood evaluations on the baselines for trajectory prediction. Based on the mean log-likelihood of the ground-truth trajectories, our method outperforms a regressor trained on this task with the same architecture as well as extrapolation from an optical flow predictor. This is reasonable since

the regressor is inherently unimodal: it is unable to predict distributions where there may be many reasonable futures, which Figs. 3 and 4 suggest is rather common. Interestingly, extrapolating the predicted optical flow from [31] does not seem to be effective, as motion may change direction considerably even over the course of one second.

(a) Negative Log Likelihood on THUMOS 2015 dataset.

Method	NLL
Regressor	11463
Optical Flow [31]	11734
Ours	<b>11082</b>



(b) Average Minimum Euclidean distance for each method per sample size

**Fig. 5.** Prediction evaluations

network predicts motion based on the context of the scene. For instance, the network tends to predict up and down motions for the people on the swing in Fig. 4, while the boy in Fig. 3 playing the violin moves his arm left and right. Figure 6 shows the role latent variables play in predicting motion in some selected scenes with a distinct action: interpolating between latent variable values interpolates between the motion prediction. Based on this figure, at least some latent variables encode the direction of motion. However, the network still depends on image information to restrict the types of motions that can occur in a scene. For instance, the man skiing moves only left or right while the woman squats only up or down.

### 4.3 Representation Learning

Prediction implicitly depends on a number of fundamental vision tasks such as recognizing the scene action and detecting the moving objects. Hence, we expect the representation learned for the task of motion prediction may generalize for other vision tasks. We thus evaluate the representation learned by our network

We plot the average minimum Euclidean distance per sample for each method in Fig. 5(b). We find that even with a small number of samples, our algorithm outperforms the baselines. The additional dashed line is the result from simply using the regressor’s direct output as a mean, which is equivalent to sampling with a variance of 0. Note that given a single sample, the regressor outperforms our method since it directly optimized the Euclidean distance at training time. Given more than a few samples, however, ours performs better due to the multimodality of the problem (Table 1).

### 4.2 Qualitative Results

We show some qualitative results in Figs. 3 and 4. For these results, we cluster 800 samples into 10 clusters via Kmeans and show top two clusters with significant motion. In our quantitative experiments, we found that the ground-truth trajectory matched into the top three clusters 75% of the time. The network

**Table 1.** mean Average Precision (mAP) on VOC 2012. The “External data” column represents the amount of data exposed outside of the VOC 2012 training set. “cal” denotes the between-layer scale adjustment [17] calibration.

VOC 2012 test	External data	aero	bike	bird	boat	bottle	bus	car	cat	chair	cow	table	dog	horse	mbike	person	plant	sheep	sofa	train	tv	mAP
scratch+cal	N/A	67.5	49.8	27.9	23.9	13.6	57.8	48.1	51.7	16.1	33.2	29.2	45.3	51.9	58.8	51.7	16.8	39.7	29.4	55.7	43.5	40.6
kmeans [17]+cal	N/A	71.1	56.8	31.8	28.1	17.7	62.5	56.6	59.9	19.9	37.3	36.2	52.9	56.4	64.3	57.1	21.2	45.8	39.1	60.9	46.0	46.1
rel. pos. [4]+cal	1.2M ImageNet	<b>74.3</b>	<b>64.7</b>	<b>42.6</b>	<b>32.6</b>	<b>25.9</b>	<b>66.5</b>	<b>60.2</b>	<b>67.9</b>	<b>27.0</b>	<b>47.9</b>	<b>41.3</b>	<b>64.5</b>	<b>63.4</b>	<b>69.1</b>	57.5	25.3	51.9	<b>46.7</b>	<b>64.6</b>	51.4	<b>52.3</b>
egomotion [1]+cal	20.5K KITTI img.	70.7	56.3	31.9	25.6	18.7	60.4	54.1	57.6	19.8	40.9	31.8	51.9	54.9	61.7	53.5	19.8	45.2	36.3	56.9	49.1	44.9
vid. embed [32]	1.5M vid. frames (100k vid)	68.8	62.1	34.7	25.3	<b>26.6</b>	57.7	59.6	56.3	22.0	42.6	33.8	52.3	50.3	65.6	53.9	<b>25.8</b>	51.5	32.3	51.7	51.8	46.2
vid. embed [32]	5M vid. frames (100k vid)	69.0	64.0	37.1	23.6	24.6	58.7	58.9	59.6	22.3	46.0	35.1	53.3	53.7	66.9	54.1	25.4	<b>52.9</b>	31.2	51.9	51.8	47.0
vid. embed [32]	8M vid. frames (100k vid)	67.6	63.4	37.3	27.6	24.0	58.7	59.9	59.5	23.7	46.3	37.6	54.8	54.7	66.4	54.8	<b>25.8</b>	52.5	31.2	52.6	<b>52.6</b>	47.5
vid. embed [32]+cal	8M vid. frames (100k vid)	68.1	53.1	31.9	24.3	16.9	57.2	50.8	58.4	14.1	36.9	27.6	52.5	49.6	60.0	48.4	15.8	41.9	34.4	55.6	45.6	42.2
ours+cal	13k UCF101 vid.	71.7	60.4	34.0	27.8	18.6	63.5	56.6	61.1	21.2	39.3	35.1	57.1	58.6	66.0	<b>58.4</b>	20.5	45.6	38.3	62.1	49.9	47.3

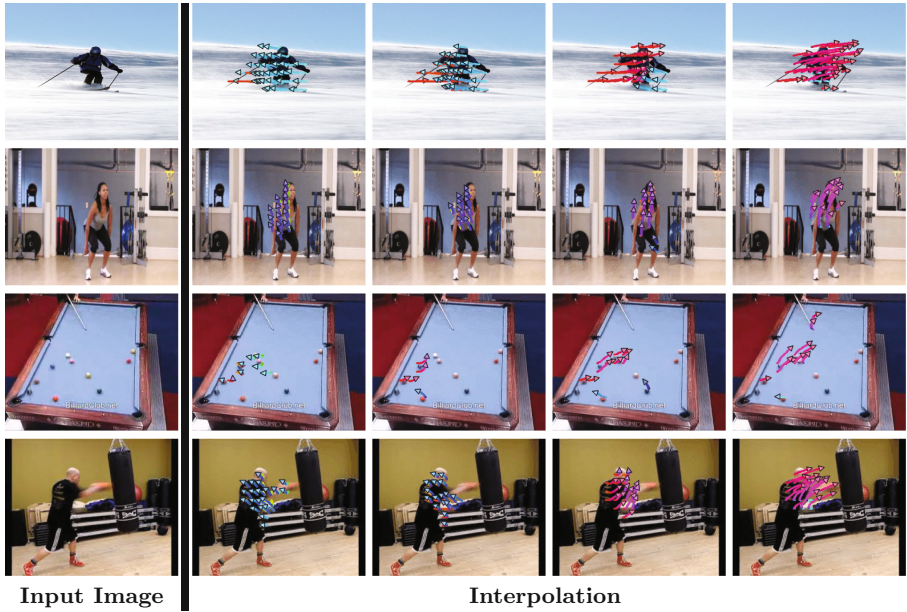


**Fig. 6.** Interpolation in latent variable space between two points from left to right. Each column represents a set of images with the same latent variables. Left to right represents a linear interpolation between two points in  $z$ -space. The latent variables influence direction to some extent, but the context of the image either amplifies or greatly reduces this direction.

on the task of object detection. We take layers from the image tower and fine-tune them on the PASCAL 2012 training dataset. For all methods, we apply the between-layer scale adjustment [17] to calibrate the pre-trained networks, as it improves the finetuning behavior of all methods except one. We then compare detection scores against other unsupervised methods of representation learning using Fast-RCNN [8]. We find that from a relatively small amount of data, our method outperforms other methods that were trained on datasets with far larger diversity in scenes and types of objects. While the improvement is small over all objects, we do have the highest performance on humans over all unsupervised methods, even [4]. This is expected as most of the moving objects in our training data comes from humans.

**Acknowledgements.** We thank the NVIDIA Corporation for the donation of Tesla K40 GPUs for this research. In addition, this work was supported by NSF grant IIS1227495.

## References

1. Agrawal, P., Carreira, J., Malik, J.: Learning to see by moving. In: ICCV (2015)
2. Baker, S., Scharstein, D., Lewis, J., Roth, S., Black, M.J., Szeliski, R.: A database and evaluation methodology for optical flow. *IJCV* **92**(1), 1–31 (2011)
3. Doersch, C.: Tutorial on variational autoencoders. arXiv preprint (2016). [arXiv:1606.05908](https://arxiv.org/abs/1606.05908)
4. Doersch, C., Gupta, A., Efros, A.A.: Unsupervised visual representation learning by context prediction. In: ICCV (2015)
5. Dosovitskiy, A., Fischer, P., Ilg, E., Hausser, P., Hazirbas, C., Golkov, V., van der Smagt, P., Cremers, D., Brox, T.: FlowNet: learning optical flow with convolutional networks. In: ICCV (2015)
6. Eigen, D., Fergus, R.: Predicting depth, surface normals and semantic labels with a common multi-scale convolutional architecture. In: ICCV (2015)
7. Fouhey, D., Zitnick, C.L.: Predicting object dynamics in scenes. In: CVPR (2014)
8. Girshick, R.: Fast R-CNN. In: ICCV (2015)
9. Gorban, A., Idrees, H., Jiang, Y.G., Roshan Zamir, A., Laptev, I., Shah, M., Sukthankar, R.: THUMOS challenge: action recognition with a large number of classes (2015). <http://www.thumos.info/>
10. Gregor, K., Danihelka, I., Graves, A., Rezende, D., Wierstra, D.: DRAW: a recurrent neural network for image generation. In: ICML (2015)
11. Hoai, M., De la Torre, F.: Max-margin early event detectors. *IJCV* **107**(2), 191–202 (2014)
12. Huang, D.-A., Kitani, K.M.: Action-reaction: forecasting the dynamics of human interaction. In: Fleet, D., Pajdla, T., Schiele, B., Tuytelaars, T. (eds.) ECCV 2014. LNCS, vol. 8695, pp. 489–504. Springer, Heidelberg (2014). doi:[10.1007/978-3-319-10584-0\\_32](https://doi.org/10.1007/978-3-319-10584-0_32)
13. Kingma, D.P., Mohamed, S., Rezende, D.J., Welling, M.: Semi-supervised learning with deep generative models. In: NIPS (2014)
14. Kingma, D.P., Welling, M.: Auto-encoding variational Bayes. In: ICLR (2014)
15. Kitani, K.M., Ziebart, B.D., Bagnell, J.A., Hebert, M.: Activity forecasting. In: Fitzgibbon, A., Lazebnik, S., Perona, P., Sato, Y., Schmid, C. (eds.) ECCV 2012. LNCS, vol. 7575, pp. 201–214. Springer, Heidelberg (2012). doi:[10.1007/978-3-642-33765-9\\_15](https://doi.org/10.1007/978-3-642-33765-9_15)
16. Koppula, H.S., Saxena, A.: Anticipating human activities using object affordances for reactive robotic response. In: RSS (2013)
17. Krähenbühl, P., Doersch, C., Donahue, J., Darrell, T.: Data-dependent initializations of convolutional neural networks. ICLR (2016)
18. Krizhevsky, A., Sutskever, I., Hinton, G.E.: Imagenet classification with deep convolutional neural networks. In: NIPS (2012)
19. Kulkarni, T., Whitney, W.F., Kohli, P., Tenenbaum, J.: Deep convolutional inverse graphics network. In: NIPS (2015)
20. Lan, T., Chen, T.-C., Savarese, S.: A hierarchical representation for future action prediction. In: Fleet, D., Pajdla, T., Schiele, B., Tuytelaars, T. (eds.) ECCV 2014. LNCS, vol. 8691, pp. 689–704. Springer, Heidelberg (2014). doi:[10.1007/978-3-319-10578-9\\_45](https://doi.org/10.1007/978-3-319-10578-9_45)
21. Liu, C., Yuen, J., Torralba, A.: Sift flow: dense correspondence across scenes and its applications. *PAMI* **33**(5), 978–994 (2011)
22. Mottaghi, R., Bagherinezhad, H., Rastegari, M., Farhadi, A.: Newtonian image understanding: unfolding the dynamics of objects in static images. In: CVPR (2016)



23. Pinteá, S.L., Gemert, J.C., Smeulders, A.W.M.: Déjà Vu: motion prediction in static images. In: Fleet, D., Pajdla, T., Schiele, B., Tuytelaars, T. (eds.) ECCV 2014. LNCS, vol. 8691, pp. 172–187. Springer, Heidelberg (2014). doi:[10.1007/978-3-319-10578-9\\_12](https://doi.org/10.1007/978-3-319-10578-9_12)
24. Ranzato, M., Szlam, A., Bruna, J., Mathieu, M., Collobert, R., Chopra, S.: Video (language) modeling: a baseline for generative models of natural videos. arXiv preprint (2014). [arXiv:1412.6604](https://arxiv.org/abs/1412.6604)
25. Rezende, D.J., Mohamed, S., Wierstra, D.: Stochastic backpropagation and approximate inference in deep generative models. In: ICML (2014)
26. Salimans, T., Kingma, D., Welling, M.: Markov chain monte carlo and variational inference: bridging the gap. In: ICML (2015)
27. Soomro, K., Zamir, A.R., Shah, M.: UCF101: A dataset of 101 human actions classes from videos in the wild. arXiv preprint (2012). [arXiv:1212.0402](https://arxiv.org/abs/1212.0402)
28. Srivastava, N., Mansimov, E., Salakhutdinov, R.: Unsupervised learning of video representations using LSTMs. In: ICML (2015)
29. Vondrick, C., Pirsiaavash, H., Torralba, A.: Anticipating the future by watching unlabeled video. In: CVPR (2016)
30. Walker, J., Gupta, A., Hebert, M.: Patch to the future: unsupervised visual prediction. In: CVPR (2014)
31. Walker, J., Gupta, A., Hebert, M.: Dense optical flow prediction from a static image. In: ICCV (2015)
32. Wang, X., Gupta, A.: Unsupervised learning of visual representations using videos. In: ICCV (2015)
33. Yuen, J., Torralba, A.: A data-driven approach for event prediction. In: Daniilidis, K., Maragos, P., Paragios, N. (eds.) ECCV 2010. LNCS, vol. 6312, pp. 707–720. Springer, Heidelberg (2010). doi:[10.1007/978-3-642-15552-9\\_51](https://doi.org/10.1007/978-3-642-15552-9_51)